Clinical Cancer Research

Discriminant Analysis of ^{18}F-Fluorothymidine Kinetic Parameters to Predict Survival in Patients with Recurrent High-Grade Glioma

Mirwais Wardak[1], Christiaan Schiepers[1], Magnus Dahlbom[1], Timothy Cloughesy[2], Wei Chen[1], Nagichettiar Satyamurthy[1], Johannes Czernin[1], Michael E. Phelps[1], and Sung-Cheng Huang[1]

Abstract

Purpose: The primary objective of this study was to investigate whether changes in 3′-deoxy-3′-[^{18}F]fluorothymidine (^{18}F-FLT) kinetic parameters, taken early after the start of therapy, could predict overall survival (OS) and progression-free survival (PFS) in patients with recurrent malignant glioma undergoing treatment with bevacizumab and irinotecan.

Experimental Design: High-grade recurrent brain tumors were investigated in 18 patients (8 male and 10 female), ages 26 to 76 years. Each had 3 dynamic positron emission tomography (PET) studies as follows: at baseline and after 2 and 6 weeks from the start of treatment, ^{18}F-FLT (2.0 MBq/kg) was injected intravenously, and dynamic PET images were acquired for 1 hour. Factor analysis generated factor images from which blood and tumor uptake curves were derived. A three-compartment, two-tissue model was applied to estimate tumor ^{18}F-FLT kinetic rate constants using a metabolite- and partial volume–corrected input function. Different combinations of predictor variables were exhaustively searched in a discriminant function to accurately classify patients into their known OS and PFS groups. A leave-one-out cross-validation technique was used to assess the generalizability of the model predictions.

Results: In this study population, changes in single parameters such as standardized uptake value or influx rate constant did not accurately classify patients into their respective OS groups (<1 and ≥1 year; hit ratios ≤78%). However, changes in a set of ^{18}F-FLT kinetic parameters could perfectly separate these two groups of patients (hit ratio = 100%) and were also able to correctly classify patients into their respective PFS groups (<100 and ≥100 days; hit ratio = 88%).

Conclusions: Discriminant analysis using changes in ^{18}F-FLT kinetic parameters early during treatment seems to be a powerful method for evaluating the efficacy of therapeutic regimens. *Clin Cancer Res; 17(20); 6553–62. ©2011 AACR.*

Introduction

In vivo imaging of cellular proliferation has tremendous potential for monitoring and predicting response to anticancer therapy. The thymidine nucleoside analogue 3′-deoxy-3′-[^{18}F]fluorothymidine (^{18}F-FLT) was developed as a molecular imaging probe to assess cellular proliferation *in vivo* with positron emission tomography (PET; ref. 1). Once ^{18}F-FLT is transported into the cell, it is phosphorylated by thymidine kinase-1 (TK-1) and subsequently trapped inside the cell (2). TK-1 is a cytosolic enzyme that is expressed during the DNA synthesis stage of the cell cycle (2). The rate-limiting step in ^{18}F-FLT accumulation is phosphorylation by TK-1, causing ^{18}F-FLT to accumulate in proportion to TK-1 activity (3). Compared with normal proliferating tissue, tumor cells have increased levels of TK-1, resulting in an increased ^{18}F-FLT uptake (4). The half-life of ^{18}F makes ^{18}F-FLT suitable for tracer kinetic analysis.

In a patient population with nontreated newly diagnosed high-grade gliomas, it was shown that kinetic modeling of ^{18}F-FLT enabled determination of tumor proliferation *in vivo* via the metabolic influx constant K_i (4). In their study, K_i strongly correlated with the proliferation index as measured by Ki-67 immunostaining, whereas uptake of methyl-^{11}C-L-methionine (^{11}C-MET) or ^{18}F-FLT failed to correlate with the *in vitro* proliferation marker Ki-67. Furthermore, a National Cancer Institute (NCI)–sponsored trial explored the capacity of ^{18}F-FLT PET to distinguish

Authors' Affiliations: Departments of [1]Molecular and Medical Pharmacology and [2]Neurology, David Geffen School of Medicine at UCLA, Los Angeles, California

Note: Supplementary data for this article are available at Clinical Cancer Research Online (http://clincancerres.aacrjournals.org/).

Corresponding Author: Sung-Cheng Huang, Department of Molecular and Medical Pharmacology, David Geffen School of Medicine at UCLA, B2-085H CHS, 10833 Le Conte Ave, Los Angeles, CA 90095. Phone: 310-825-6647; Fax: 310-825-4517; E-mail: hhuang@mednet.ucla.edu

doi: 10.1158/1078-0432.CCR-10-3290

©2011 American Association for Cancer Research.

Downloaded from http://aacrjournals.org/clincancerres/article-pdf/17/20/6553/2000121/6553.pdf by guest on 19 June 2024

Translational Relevance

Conventional MRI techniques are commonly used in the diagnosis and follow-up of patients with malignant glioma. However, in many situations, changes in contrast enhancement on standard MRI do not correlate with treatment response. Advanced imaging methods are therefore needed to overcome the limitations of conventional MRI. In this positron emission tomography study, we investigated whether changes in 3′-deoxy-3′-[^{18}F]fluorothymidine kinetic parameters, at 2 and 6 weeks after the start of treatment, could predict overall survival and progression-free survival in patients with recurrent malignant glioma undergoing treatment with bevacizumab and irinotecan. This article shows that when a group of optimal kinetic parameter changes are incorporated into a linear discriminant function, one could accurately classify patients into their known survival groups. This method is advantageous because by reliably identifying short- and long-term survivors early during therapy, clinicians can discontinue ineffective treatment strategies and switch to more advanced treatment regimens that could improve patient outcome.

recurrence from radiation necrosis in previously treated gliomas (5). In the NCI trial, it was shown that K_i and the phosphorylation rate constant k_3 seemed to distinguish tumor recurrence from radiation necrosis, with the clinical diagnosis determined independently after the ^{18}F-FLT PET scan (5). Standardized uptake value (SUV) and visual analyses of ^{18}F-FLT or 2-^{18}F-fluoro-deoxy-D-glucose (^{18}F-FDG) images did not significantly separate the 2 groups in the NCI trial. Kinetic modeling with ^{18}F-FLT and other molecular imaging probes in brain tumor patients has also been reported elsewhere (6–10). In the evaluation of treatment response, ^{18}F-FLT was used in a group of patients with recurrent glioma who received a combination of antiangiogenic and chemotherapeutic agents (11). A reduction of more than 25% in tumor SUV, defined as a metabolic response, was found to be the threshold with the best predictive power for overall survival (OS; ref. 11). Treatment response in patients with brain tumors has also been assessed by other PET tracers (12–14) and with advanced MRI techniques (15, 16).

The primary purpose of this work was to investigate whether changes in ^{18}F-FLT kinetic parameters, taken early after the start of therapy, could predict OS and progression-free survival (PFS) in patients with recurrent malignant glioma undergoing treatment with bevacizumab and irinotecan. We hypothesized that there exists a group of kinetic parameter changes that when incorporated into a linear discriminant function would be able to accurately distinguish short-term survivors from long-term survivors. We also hypothesized that this set of parameter changes would provide more predictive information than ^{18}F-FLT uptake changes alone.

Materials and Methods

Study participants

The studied population consisted of 18 patients with recurrent high-grade glioma. Fifteen of the 18 patients were from our previous study (10) and 3 were newly enrolled. The time period during which the data were collected was from July 2005 to June 2009. There were 8 men and 10 women, with a mean age of 54 ± 15 years (range: 26–76 years) at the start of the study. All gliomas were confirmed by histopathology and graded according to the World Health Organization scheme. Sixteen patients had glioblastoma multiforme (GBM; grade IV), 1 patient had anaplastic astrocytoma (grade III), and 1 patient had anaplastic mixed glioma (AMG; grade III). Each patient had previously undergone surgical resection followed by adjuvant treatment with chemotherapy and/or radiation. The median number of prior treatments was 1 (range: 1–3). An overview of the population data is shown in Table 1. In accordance with the procedures of the Office of the Human Research Protection Program at UCLA, written informed consent was obtained from all subjects.

Treatment

Patients were treated off-label with biweekly cycles of bevacizumab (10 mg/kg) and irinotecan (125 or 350 mg/m^2 depending on concomitant use of enzyme-inducing antiepileptic drugs). Bevacizumab is a recombinant humanized monoclonal antibody that binds to and inhibits the activity of VEGF. Irinotecan is a chemotherapeutic agent that inhibits topoisomerase I, an enzyme that helps unwind DNA during replication. All 18 enrolled patients finished the first course of 6 weeks. No patient was lost to follow-up.

Patient outcome

Patients had regular follow-up at the Neuro-Oncology Clinic, and the date of progression was diagnosed by the neuro-oncologist on the basis of physical examination, clinical deterioration, and imaging. PFS was calculated from the date of baseline ^{18}F-FLT PET to the date of disease progression. In data pooled from 16 clinical trials that used various pharmaceuticals in treating patients for recurrent GBM (none of which included bevacizumab), the median PFS was 1.8 months (17). Because most tumors in our patient population were GBM (16 of 18; 89%), we selected 100 days as a reasonable cutoff point for patients with rapid recurrence versus usual disease progression. OS was calculated from the date of baseline ^{18}F-FLT PET to the date of patient death. A cutoff value of 1 year for OS (17) was used to distinguish short-term survivors from long-term survivors.

^{18}F-FLT synthesis

^{18}F-FLT was synthesized according to the method developed by Walsh and colleagues (18). The chemical and

Downloaded from http://aacrjournals.org/clincancerres/article-pdf/17/20/6553/2000121/6553.pdf by guest on 19 June 2024

Table 1. Clinical characteristics of all patients

Patient No.	Sex	Age, y	Pathology at recurrence	WHO grade at recurrence	Initial therapy	Prior treatments	Time from initial diagnosis,[a] d	PFS, d	OS, d
1	M	50	AA	3	Chemotherapy/XRT	2	332	29	59
2	M	69	GBM	4	Chemotherapy/XRT	1	76	81	81
3	F	65	GBM	4	Chemotherapy/XRT	2	578	78	107
4	F	59	GBM	4	Chemotherapy/XRT	1	322	42	169
5	M	64	GBM	4	Chemotherapy/XRT	1	178	70	234
6	F	37	AMG	3	Chemotherapy/XRT	1	160	155	260
7	M	37	GBM	4	Chemotherapy	2	4,225	62	292
8	M	68	GBM	4	Chemotherapy/XRT	2	332	218	315
9	F	35	GBM	4	XRT	3	2,804	65	318
10	F	54	GBM	4	Chemotherapy/XRT	1	91	226	343
11	M	45	GBM	4	Chemotherapy/XRT	1	132	74	344
12	M	26	GBM	4	Chemotherapy	3	462	96	364
13	F	40	GBM	4	Chemotherapy/XRT	1	462	44	366
14	F	47	GBM	4	Chemotherapy/XRT	1	160	176	374
15	F	70	GBM	4	Chemotherapy/XRT	1	362	184	395
16	F	61	GBM	4	Chemotherapy/XRT	2	719	137	400
17	F	62	GBM	4	Chemotherapy/XRT	1	316	273	709
18	M	76	GBM	4	Chemotherapy/XRT	1	134	978	978

Abbreviations: PFS, progression-free survival; OS, overall survival; AA, anaplastic astrocytoma; XRT, radiation therapy.
[a]Time from initial diagnosis is the number of days from initial diagnosis to start of treatment in the current study.

radiochemical purities of ^{18}F-FLT were found to be more than 99%. The specific activity of ^{18}F-FLT was more than 1,000 Ci/mmol (>37 TBq/mmol). The final product was sterile and pyrogen free.

Imaging protocol

The study protocol was approved by the UCLA Institutional Review Board, the UCLA Medical Radiation Safety Committee, and the UCLA Radioactive Drug Research Committee. A baseline ^{18}F-FLT PET [study 1 (S1)] was carried out within 1 week before the start of treatment, and follow-up ^{18}F-FLT scans were carried out at 2 weeks [study 2 (S2)] and then again at 6 weeks [study 3 (S3)] after the start of treatment. The experimental design is illustrated in Fig. 1. PET imaging was carried out with an ECAT EXACT HR+ scanner (Siemens/CTI). The intrinsic spatial resolution of the scanner was 4.5 mm full-width at half-maximum (FWHM) in the center of the field of view. Using a set of

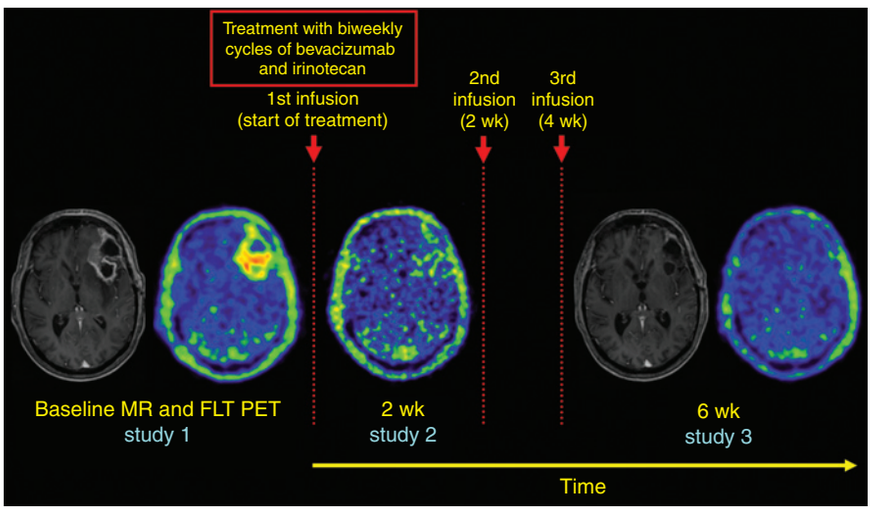

Figure 1. Experimental design used in this study. A baseline ^{18}F-FLT PET was carried out within 1 week before the start of treatment, and follow-up ^{18}F-FLT PET scans were carried out at 2 weeks and then again at 6 weeks after the start of treatment. Shown on the right are summed ^{18}F-FLT PET images (50–60 minutes) and their corresponding contrast-enhanced T1-weighted MRIs. No MRI was carried out at 2 weeks. ^{18}F-FLT PET images at 2 and 6 weeks were coregistered to the baseline PET, and the 6-week MRI was aligned to the coregistered baseline MRI. Images are displayed using the same color scale within each modality. The patient shown here was a long-term survivor.

Downloaded from http://aacrjournals.org/clincancerres/article-pdf/17/20/6553/2000121/6553.pdf by guest on 19 June 2024

external rotating ^{68}Ge/^{68}Ga rod sources, a transmission scan was first acquired for 5 minutes in 2-dimensional mode to correct for photon attenuation. Subsequently, 2.0 MBq/kg of ^{18}F-FLT was injected intravenously as a bolus, and a dynamic emission scan with 23 frames (8 × 15, 2 × 30, and 2 × 60 seconds and 11 × 5 minutes) was acquired in 3-dimensional mode. PET emission data were reconstructed using ordered subset expectation maximization (6 iterations and 16 subsets) with a zoom factor of 2.5. A Gaussian kernel of 5-mm FWHM was used as a postreconstruction smoothing filter. The spatial resolution of the final reconstructed images was 6.7-mm FWHM. The final reconstructed volume had a matrix size of 128 × 128 and consisted of 63 planes, resulting in a voxel size of 2.06 × 2.06 × 2.425 mm^3.

Factor analysis

Factor analysis (19, 20) generated factor images from which blood and tumor uptake curves were derived. Briefly, the factor model assumes that in a dynamic image there are groups of voxels that have the same time behavior (21). In our implementation, 3 factor images (representing the brain vessels, tumor, and the rest) were generated. A 50% threshold of the maximum voxel in the vascular factor image (transverse and cavernous sinuses) was used to create a volume-of-interest (VOI) that would extract the blood time–activity curve (TAC) when overlaid on the dynamic PET image. The tumor TAC was extracted using a 75% threshold of the tumor factor image to get the most proliferative part of the tumor. Necrotic zones have low ^{18}F-FLT uptake and, therefore, do not reach the threshold of 75% uptake of the tumor maximum. Areas with necrosis (e.g., centrally "cold" tumors) were thus explicitly excluded during the VOI creation. The effects of using varying isocontours have been investigated earlier (10). The measured blood and tumor TACs were then used for kinetic modeling analysis.

^{18}F-FLT compartmental model

The standard 3-compartment, 2-tissue model for ^{18}F-FLT is analogous to that of ^{18}F-FDG and is illustrated in Supplementary Fig. S1. After intravenous injection, ^{18}F-FLT is transported across the cell membrane by sodium-dependent (concentrative) and sodium-independent (equilibrative) nucleoside transporters (22). The transport of ^{18}F-FLT from the plasma compartment (C_p) into the exchangeable tissue compartment (C_E), as it crosses the disrupted blood–brain barrier (BBB), is represented by the rate constant K_1 (mL/cm^3/min). The exchangeable tissue compartment represents ^{18}F-FLT in its intact, nonphosphorylated state. ^{18}F-FLT glucuronide, a metabolite that accumulates in the blood over time when ^{18}F-FLT is metabolized by the liver, does not cross into the exchangeable tissue compartment (i.e., it is restricted to the vascular space). Furthermore, it has been shown that there is no partitioning in the vascular space and that plasma and whole blood activity concentrations are the same (23, 24). The return of ^{18}F-FLT from the exchangeable tissue compartment back into the plasma compartment is represented by the rate constant k_2 (min^{-1}).

At the intracellular level, ^{18}F-FLT in the exchangeable compartment is phosphorylated by TK-1 to produce the nucleotide ^{18}F-FLT monophosphate and, to a limited degree, the di- and triphosphate forms as well (2). The metabolic trapping of ^{18}F-FLT via the phosphorylation step is represented by the rate constant k_3 (min^{-1}). ^{18}F-FLT nucleotides in the trapped compartment (C_M) are not incorporated into DNA (2). However, ^{18}F-FLT nucleotides in the trapped compartment can be dephosphorylated back into the exchangeable compartment, as represented by the rate constant k_4 (min^{-1}).

The differential equations that describe the rate of change of ^{18}F-FLT concentration in each of the tissue compartments can be solved with the use of Laplace transforms with their solutions shown in ref. 25. Kinetic modeling yields 4 rate constants K_1, k_2, k_3, and k_4 and an estimated fifth parameter, the blood volume fraction (V_b), which is the fraction of vascular space in the tumor VOI. For brain tumor regions where the BBB is disrupted, V_b contains some interstitial space as well. From these 5 estimated microparameters, certain physiologically important macroparameters can be calculated, such as the influx rate constant $\left[K_i = \frac{K_1 \times k_3}{k_2 + k_3}\right]$, the volume of distribution $\left[V_d = \frac{K_1}{k_2 + k_3}\right]$, and the phosphorylated fraction $\left[\mathrm{PF} = \frac{k_3}{k_2 + k_3}\right]$. PF is the fraction of ^{18}F-FLT transported via K_1 that ends up in the phosphorylated ^{18}F-FLT pool. In addition, ^{18}F-FLT uptake measurements (expressed as SUVs) were calculated at early (from 10 to 25 minutes) and late time points (from 50 to 60 minutes).

Metabolite and partial volume corrections

Blood metabolites were not measured in this study. Metabolites in the blood were corrected by subtracting a metabolite fraction from the blood TAC as explained in our previous publication (7). The equation for the metabolite fraction over time was calculated as $0.42 \times (1 - e^{-0.029 \times t})$. A recovery coefficient of 0.7 was chosen to convert the image-based measured blood TAC to the input function (7). Because the tumors were relatively large (>15 mm) compared to the image resolution, the recovery coefficient of the output function was set to unity (7).

Statistical analysis

The Mann–Whitney *U* test was used for between-group comparisons for all absolute parameters (at each study time point) and their relative changes (between each study time point). For paired samples, the Wilcoxon signed-rank test was applied. Spearman correlations were computed to assess the association between 2 variables. All statistical analyses were performed using SPSS (version 19.0; IBM Corporation). The results are reported as the mean ± SD (unless otherwise noted) and are regarded as statistically significant if $P < 0.05$.

Discriminant analysis

Given a common set of variables for 2 or more groups of individuals, discriminant analysis attempts to find linear

Downloaded from http://aacrjournals.org/clincancerres/article-pdf/17/20/6553/2000121/6553.pdf by guest on 19 June 2024

combinations of those variables that best separate each group (26). These combinations are called discriminant (or classification) functions and have the form displayed as in Equation (A).

$$D = b_1x_1 + b_2x_2 + \ldots + b_nx_n + C \quad \text{(A)}$$

where D is the discriminant score formed by the discriminant function, b_n are the unstandardized discriminant coefficients, x_n are the predictor variables, and C is a constant. The values of the coefficients are chosen so that the discriminant scores of individuals in any group have the smallest possible variance and, at the same time, the difference between the average discriminant scores of the 2 groups is as big as possible (26). A graphical representation of the predictive technique is shown in Supplementary Fig. S2.

In this study, a discriminant function was generated on the original sample of 18 subjects for which group membership was known. All possible predictor combinations were exhaustively searched to maximize a test statistic called the Wilks λ (27). To produce a nearly unbiased estimate of the proportion misclassified, a leave-one-out cross-validation procedure was carried out whereby each subject was excluded and then classified with the use of the discriminant function based on the remaining subjects (26). For each predictor combination, the classification accuracies of the original grouped cases and the cross-validated grouped cases were computed. The Press's Q statistic was used to determine whether the discriminatory power of the classification model was statistically better than chance (27).

Results

Outcome analysis

Table 1 summarizes the clinical characteristics of all patients. At the time of writing this article, all patients had died and therefore all variables (clinical and imaging based) were known. Patients in the original sample ($n = 18$) were designated into 2 groups with regard to their OS and PFS and the cutoff points of 1 year and 100 days, respectively (as detailed under Patient Outcome). From here on, the groups for OS will be referred to as Short-OS and Long-OS and the groups for PFS will be referred to as Short-PFS and Long-PFS. The median OS and PFS for the entire sample were 330.5 days (11.0 months) and 88.5 days (2.95 months), respectively. The median OS for Short-OS ($n = 12$) and Long-OS ($n = 6$) was 276 and 398 days (9.2 and 13.3 months), respectively. The median PFS for Short-PFS ($n = 9$) and Long-PFS ($n = 8$) was 70 and 201 days (2.3 and 6.7 months), respectively. Patient 1 from Table 1 was not included in the PFS analysis because this patient's tumor progressed before the 6-week PET measurement. OS and PFS were shown to be correlated (Spearman's $\rho = 0.62$; $P < 0.007$).

Factor analysis

Supplementary Figure S3 shows the vascular and tumor factor images along with the measured blood and tumor TACs. Three-dimensional movies of the factor images can be found in the Supplementary Data section.

Tumor kinetics and SUV

Mean ^{18}F-FLT SUVs for Short-OS and Long-OS at each of the 3 study time points are shown as bar graphs in Supplementary Fig. S4. Similar graphs for the 2 patient groups are shown in Supplementary Fig. S5 for various kinetic parameters and V_b (unitless).

At each study time point, detailed inspection of the absolute values of kinetic and SUV parameters revealed no significant group differences between Short-OS and Long-OS and between Short-PFS and Long-PFS; therefore, relative changes were calculated and analyzed. The percentage of change in SUV from S1 → S2 $\left[\frac{(S2-S1)}{S1}\right] \times 100\%$, S1 → S3, and S2 → S3 is shown for both Short-OS and Long-OS in Supplementary Table S1. The percentage of change in kinetic and derived parameters from S1 → S3 is shown in Table 2, whereas those from S1 → S2 and S2 → S3 are shown in Supplementary Tables S2 and S3, respectively. From S1 → S2, SUV (early and late) and K_i decreased for both Short-OS and Long-OS. However, from S2 → S3, Short-OS increased in their SUV and K_i values whereas Long-OS continued to decrease in their SUV and K_i values. A slightly different scenario played out for k_3 and PF. From S1 → S2, k_3 and PF increased for both Short-OS and Long-OS. However, from S2 → S3, Short-OS continued to increase in their k_3 and PF values whereas Long-OS decreased in their k_3 and PF values.

The Wilcoxon signed-rank test was used for evaluating the within-group differences before and after the start of treatment. For Short-OS, significant paired sample differences were found for K_1, K_i, V_d, and SUV (early and late) from S1 → S2, and for V_d and SUV_{early} from S1 → S3. No significant paired sample differences were found from S2 → S3 for Short-OS. For Long-OS, significant paired sample differences were found for V_b and SUV (early and late) from S1 → S2, and for K_i and SUV (early and late) from S1 → S3. No significant paired sample differences were found from S2 → S3 for Long-OS.

For Short-PFS, significant paired sample differences were found for K_1, K_i, and SUV (early and late) from S1 → S2 and for K_i and SUV_{late} from S2→S3. No significant paired sample differences were found from S1 → S3 for Short-PFS. For Long-PFS, significant paired sample differences were found for K_1, V_b, K_i, V_d, and SUV (early and late) from S1 → S2 and for K_i and SUV (early and late) from S1 → S3. No significant paired sample differences were found from S2 → S3 for Long-PFS.

When analyzing the relative changes between studies, several significant between-group differences were revealed by the Mann–Whitney U test. The change in blood volume fraction (ΔV_b) from S1 → S2, the change in influx rate constant (ΔK_i) from S1 → S3, and the changes in k_3, K_i, and PF from S2 → S3 were shown to be statistically significant between Short-OS and Long-OS. With regard to PFS, no significant group differences were found for all the various kinetic and SUV changes from S1 → S2. However, the

Downloaded from http://aacrjournals.org/clincancerres/article-pdf/17/20/6553/2000121/6553.pdf by guest on 19 June 2024

Table 2. Percentage of change in ^{18}F-FLT kinetic parameters (baseline → 6 weeks)

Patient No.	ΔK_1	Δk_2	Δk_3	Δk_4	ΔV_b	ΔK_i	ΔV_d	ΔPF
Short-OS								
1	–52	–29	–30	14	9	–52	–32	0
2	–28	–24	47	126	265	12	–23	56
3	137	2	–55	–44	5	24	177	–48
4	–60	–42	86	176	–7	–22	–58	94
5	–51	–20	20	2	–20	–35	–46	31
6	–8	–26	–26	8	–22	–7	24	0
7	–68	–79	55	–30	–84	2	–34	216
8	–71	–61	–64	–77	–10	–72	–23	–4
9	–68	–74	7	50	54	–32	–36	111
10	13	354	281	159	0	2	–73	–9
11	–20	56	55	–9	–15	–20	–49	0
12	39	40	60	–20	–29	53	–4	11
Mean ± SD ($n = 12$)	–20 ± 60	8 ± 116	36 ± 91	30 ± 82	12 ± 86	–12 ± 34	–15 ± 65	38 ± 72
Long-OS								
13	–40	–48	–56	–50	–53	–48	20	–12
14	–50	–62	–63	–43	–39	–50	35	–1
15	105	120	–48	–16	–44	–40	14	–71
16	5	174	90	3	–62	–22	–59	–25
17	–17	8	–26	–2	–2	–40	–18	–27
18	–90	–84	–21	25	21	–74	–67	160
Mean ± SD ($n = 6$)	–15 ± 67	18 ± 106	–21 ± 57	–14 ± 29	–30 ± 32	–46 ± 17	–13 ± 43	4 ± 80

change in K_i from S1 → S3 and the changes in k_3, K_i, and PF from S2 → S3 were shown to be statistically significant between Short-PFS and Long-PFS.

Classification using SUV

Reductions in SUV (early and late) of more than 25% from S1 → S2 and S1 → S3 were used as one method (11) to classify patients into their known OS group membership (<1 or ≥1 year). A reduction in SUV_{early} of more than 25% from S1 → S2 yielded the best results with a classification accuracy (or hit ratio) of 56% (10 of 18; Fig. 2A).

In another approach, when a change in SUV (early and late) from S1 → S2, S1 → S3, or S2 → S3 was used as a single-predictor variable in a discriminant function, ΔSUV_{early} from S2 → S3 and ΔSUV_{late} from S2 → S3 yielded the best results with hit ratios of 78% (14 of 18) each. ΔSUV_{late} from S1 → S3 yielded the next best classification result with a hit ratio of 56% (10 of 18).

Classification using kinetic information

Table 3 summarizes the discriminant functions (DF1 and DF2) that best classify the 18 patients into their respective OS (<1 or ≥1 year) and PFS (<100 or ≥100 days) groups using an optimal group of ^{18}F-FLT kinetic parameter changes. The predictor variables are shown in descending rank order in terms of their standardized coefficients. None of the discriminating variables in DF1 and DF2 were found to be significantly correlated with each other.

The classification results showed that DF1 correctly predicted 100% (18 of 18) of the original sample into their appropriate OS groups (Wilks $\lambda = 0.264$, $\chi^2_4 = 18.65$; $P = 0.001$). With cross-validation, the classification accuracy was 94% (17 of 18). The discriminant scores of each individual using DF1 are shown in Fig. 2B. Furthermore, if a change in K_i was used as the only predictor variable in the discriminant function, ΔK_i from S2 → S3 yielded the best results with a hit ratio of 78% (14 of 18). ΔK_i from S1 → S3 yielded the next best classification result with a hit ratio of 72% (13 of 18).

For PFS, the results showed comparable performance. The classification results indicated that DF2 correctly predicted 88% (15 of 17) of the original sample into their appropriate PFS groups (Wilks $\lambda = 0.402$, $\chi^2_3 = 12.30$; $P = 0.006$). With cross-validation, the classification accuracy remained at 88%. The discriminant scores of each individual using DF2 are shown in Fig. 3. In addition, the Press's Q statistic showed that the discriminant models of DF1 and DF2 performed significantly better than pure chance expectations ($P < 0.005$).

Discussion

To correctly predict the treatment response of a patient with cancer, it is prudent to collect as much biological/functional information about the patient's tumor before and after the start of treatment. Kinetic modeling in PET can provide such information. Instead of being limited to looking at just one part of the tumor biology, kinetic modeling with dynamic PET data can give us a better view of what is going on with the tumor dynamics as a whole.

Downloaded from http://aacrjournals.org/clincancerres/article-pdf/17/20/6553/2000121/6553.pdf by guest on 19 June 2024

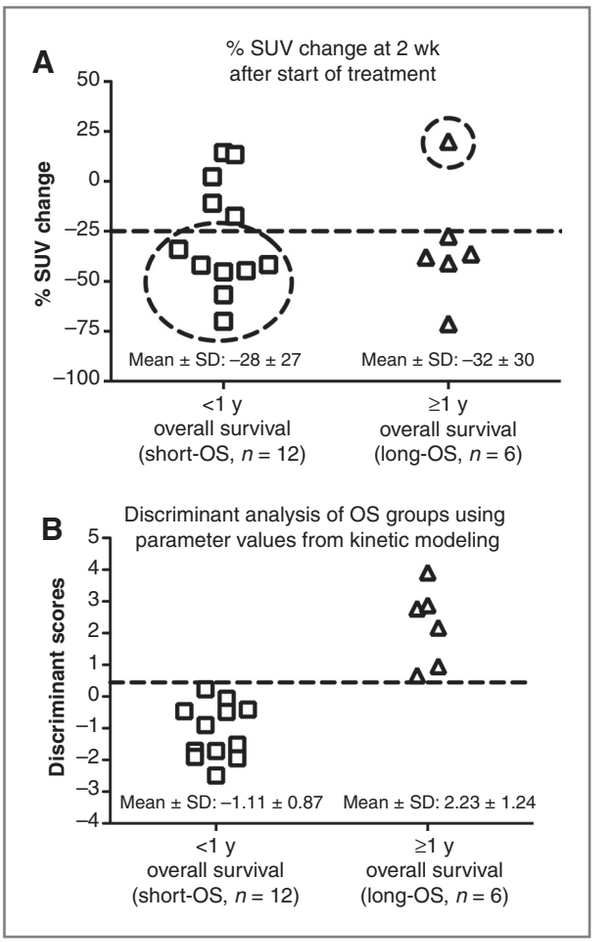

Figure 2. A, using a reduction in SUV_{early} of more than 25% after 2 weeks from the start of treatment correctly classified 10 of 18 patients. With this SUV reduction criterion, 7 patients in Short-OS would be misclassified as long-term survivors and 1 patient in Long-OS would be misclassified as a short-term survivor. B, discriminant analysis using changes in ^{18}F-FLT kinetics could correctly classify all 18 patients in their true OS group. Note the complete separation of the discriminant scores between the 2 groups.

That is why PET is such a powerful tool for studying the biology of human disease (25, 28).

In this study, changes in ^{18}F-FLT kinetic parameters, taken at an early stage after the start of therapy, were used in a linear discriminant function to stratify clinical outcome in 18 patients with recurrent brain tumor. We showed that with this method, we could accurately classify the patient population into their respective OS and PFS groups with classification accuracies of 100% and 88%, respectively. It was the relative changes in ^{18}F-FLT kinetic parameters and not their absolute values that were of importance to the group classification. The leave-one-out cross-validation technique, which was a measure of robustness of the discriminant function, provided classification results that were also comparable. Taken together, these findings indicate that the proportion of variance in the discriminant functions explained by the predictor variables that define group membership was significantly high. Moreover, the kinetic analysis is completely image based and virtually operator independent.

Table 3. Discriminant functions for classifying patients into their respective OS and PFS groups using ^{18}F-FLT kinetic information

Predictor variables	Unstandardized coefficients	Standardized coefficients
Discriminant function for OS (DF1)		
ΔK_1 (S1 → S2)	3.994	1.101
ΔK_i (S1 → S3)	–3.175	–0.951
ΔPF (S1 → S2)	1.311	0.940
ΔV_b (S1 → S2)	–3.019	–0.813
Constant	–0.364	–
Discriminant function for PFS (DF2)		
ΔPF (S2 → S3)	3.309	1.230
ΔK_1 (S2 → S3)	1.250	0.988
ΔV_b (S2 → S3)	0.640	0.637
Constant	–0.740	–

The discriminant functions for OS and PFS included a parsimonious group of predictor variables that produced excellent classification results. The changes in K_1, PF, and V_b from S1 → S2 as well as the change in K_i (includes K_1 and k_3) from S1 → S3 were shown to be a powerful set of predictor variables for classifying patients into their respective known OS groups. For predicting PFS group membership, the changes in PF, K_1, and V_b from S2 → S3 were shown to be a good set of classification variables. The predictor variables in the discriminant functions for OS and PFS were not the same, which seems reasonable because the cause of disease progression at 100 days is presumably different

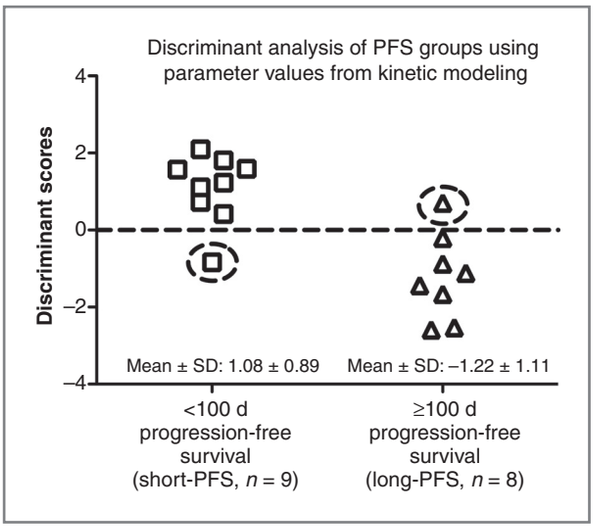

Figure 3. Discriminant analysis using changes in ^{18}F-FLT kinetics could correctly classify PFS group membership for 15 of 17 patients. Patient 1 from Table 1 was not included in the analysis, because tumor progression occurred before the 6-week PET measurement.

Downloaded from http://aacrjournals.org/clincancerres/article-pdf/17/20/6553/2000121/6553.pdf by guest on 19 June 2024

from the cause of death at 1 year. In addition, the tumor cell biology could change during the course of therapy. The predictor variables were not highly correlated within each function, indicating that they shared little redundant information in the group classification.

The predictor variables in the discriminant functions have biological relevance as well. ΔK_i (S1 → S3) reflects the overall proliferation difference between the short-term and long-term survivors [ΔK_i (S1 → S3) decreases more in the long-term survivors; ref. 10]. About a biological explanation for ΔK_1 (S1 → S2), ΔPF (S1 → S2), and ΔV_b (S1 → S2), one could speculate on the following 2 levels.

First, normalization of the neovascularization by bevacizumab. Patients responding more favorably are expected to show a larger decrease in V_b, which is what we found. Transient normalization of the tumor vasculature could also enhance the delivery of administered cytotoxic agents (29). It has been previously shown that TK-1 is upregulated in response to DNA damage caused by genotoxic insults in tumor cells (30, 31). Irinotecan and its more potent metabolite, SN-38, are known to induce single- and double-stranded DNA breaks (32). This may be the early scenario with the tumors of the long-term survivors before they eventually succumb to the cytotoxic effects of additional chemotherapy. This would explain the larger initial increase in ΔPF and Δk_3 from S1 → S2 for the long-term survivors.

Second, changes in the permeability of the vasculature and the tumor. Aggressive tumors most likely have a "leaky BBB" when compared with lower grade tumors. This explains why the baseline transport rate K_1 was high. If the therapy is able to restore a more "normal" situation, the K_1 value is expected to decrease as our data showed.

However, if the tumor has a K_1 value for the therapeutic agent that decreases less from S1 → S2, then the patient is expected to be a long-term survivor, as the intracellular concentration of the drug is, on average, higher in patients with a favorable outcome. For the short-term survivors, the tumors have probably figured out how to get rid of the toxins (and ^{18}F-FLT) by pumping them out or preventing them from entering the cell [thus, ΔK_1 (S1 → S2) decreases more]. In the above, it is assumed that changes in the transport rate constant K_1, as measured by ^{18}F-FLT, is similar for the chemotherapeutic agent. This assumption is based on previous studies that have shown that certain multidrug transporters in the BBB (e.g., MRP4 and BCRP) are known to transport camptothecin derivatives (such as irinotecan) and some nucleoside analogues such as azidothymidine and FLT (33, 34). The net effect on refractory tumors is that the initially observed change in K_i (from S1 → S2) returns to its baseline value for the third study S3, whereas the patients who benefit from the therapy show a further decrease in K_i.

It is important to note that discriminant analysis can be determined at 6 weeks after the start of treatment, which can be months to more than a year before final outcome. This offers the possibility that ^{18}F-FLT PET could replace PFS as a surrogate endpoint for OS, considered the gold standard primary efficacy endpoint. However, further prospective studies would be needed to confirm this assertion. The results of this study show that kinetic modeling in PET can extract important molecular and biochemical information inherent to the tumor, which can be used to reliably distinguish patients who will respond favorably to a certain therapy (long-term survivors) from those who will not (short-term survivors).

In this patient population, changes in a single parameter, whether incorporated into a discriminant function as the sole predictor variable or using a more than 25% reduction criterion in the case of SUV, did not accurately classify patients into their known OS groups (hit ratios $\leq$78%). The reason for this is that there is less information about the tumor biology using just one-parameter change. A recent study (10) showed that a special subgroup of long-term survivors ($n = 5$) was found within their patient sample ($n = 15$) in which the SUV (early and late) for every patient in that group dropped by more than 25% (JCO 2007 criterion; ref. 11) from S1 → S2 and S1 → S3. However, these single-parameter changes (used in and of themselves) also misclassified the short-term survivors in their study (10), which is a situation that one may not be willing to tolerate. In contrast to these results, this article shows that the misclassification error of the short-term survivors is greatly reduced when a select group of kinetic parameter changes are used in a linear discriminant function. By including more biological information about the tumor, the discriminant function provides greater confidence in the survival (and therefore treatment response) prediction for each patient.

Unlike the JCO article (11), no PET criterion was defined beforehand to categorize the patient's response to treatment. Our current study dealt with outcome analysis. The OS of the patients was used to categorize the data. SUV and kinetic information could also be integrated in the discriminant function analysis. Our study was different from the NCI-sponsored trial (5) as well. In their study, no statistical tool or criterion was provided to predict OS or PFS. Their main focus was using baseline ^{18}F-FLT kinetic parameters to distinguish recurrence from radiation necrosis. The treatment administered after the single ^{18}F-FLT PET scan in the NCI trial was also different from our study.

Other investigators have similarly used advanced imaging and quantitative techniques to assess treatment response in patients with glioma. Studies from Galldiks and colleagues (12) and Wyss and colleagues (14) showed that after temozolomide chemotherapy, PET imaging with ^{11}C-MET and ^{18}F-labeled O-(2)-fluoro-ethyl-L-tyrosine could detect responses after 3 months in high-grade and low-grade gliomas. From these findings, the deactivation of amino acid transport seemed to be an early indicator of chemotherapy response. Pope and colleagues (15) reported that for 41 bevacizumab-treated patients with recurrent GBM, apparent diffusion coefficient histogram analysis on "pretreatment" diffusion-weighted MRI could predict a 6-month PFS or greater with 73% accuracy.

This was a small exploratory study with limitations. For example, the discriminant function used to predict OS group membership required kinetic information extracted

Downloaded from http://aacrjournals.org/clincancerres/article-pdf/17/20/6553/2000121/6553.pdf by guest on 19 June 2024

from 3 dynamic PET studies. This may be inconvenient for the patient. If 2 imaging studies are done rather than 3, the hit ratio would drop from 100% to 89%, with the function using changes from S1 → S3 performing better than those using changes from S1 → S2 or S2 → S3. A larger study is warranted to confirm the predictive efficacy of the discriminant functions presented in this article. Furthermore, it is cautioned that if the estimated discriminant functions are used to classify individuals in the future, it is important that the future sample comes from a population similar to the one the discriminant functions were computed on.

Blood metabolites were not measured in this study, but corrections were applied using a model approach. Patients treated with chemotherapy may have altered liver function that could affect the metabolism of ^{18}F-FLT. If liver function were impaired, we would overestimate the true metabolite fraction, which would lead to a higher value in K_i. Because K_i is a composite parameter, this would lead to higher values in K_1 and k_3 and to a lower value in k_2. Underestimation of the true metabolite fraction would have the opposite effect. Nevertheless, this is a limitation of our study that still needs to be addressed in future experiments.

The cutoff points for PFS and OS were chosen as 100 days and 1 year, respectively, based on the article of Ballman and colleagues (17), where it was shown that these seemed as reasonable initial cutoff points for discriminant analysis. Previous results from an analysis of 12 phase II clinical trials conducted by the North American Brain Tumor Consortium showed that progression status at 2, 4, and 6 months (measured from time of registration) predicted subsequent survival time for patients with recurrent high-grade glioma (35). In our patient population, 3 patients had died within 3.5 months and 4 had died within 6 months. The median PFS and OS for the entire sample were shown to be 3 and 11 months, respectively. Although not carried out here, discriminant functions could just as well have been computed at other PFS and OS cutoff times, providing an even clearer interval of patient survival.

Future work can extend the statistical analysis to multiple linear regression, where the inputs will still be the relative changes in ^{18}F-FLT kinetic parameters but the output, instead of being a dichotomous categorical variable, will now be a continuous variable (i.e., each patient will get a numerical estimate of their survival time). Multimodality imaging parameters could also be implemented as added information about the tumor biology. Although we focused on patients with recurrent brain tumor using ^{18}F-FLT PET, the same methods presented in this study can be potentially applied to other molecular imaging probes and to other types of cancers undergoing different treatments, making the future of kinetic modeling in nuclear medicine and oncology exciting and promising.

Conclusions

Discriminant analysis using changes in ^{18}F-FLT kinetics after the start of treatment seems to be a powerful method for evaluating the efficacy of therapeutic regimens and could potentially replace PFS as a surrogate endpoint for OS. This is advantageous because by being able to determine whether a specific treatment is working shortly after its administration, clinicians can personalize therapy for each patient and decrease possible harmful side effects. Kinetic modeling with dynamic PET data may play an integral role in a clinician's assessment of treatment response, as it can extract pharmacokinetic signatures during the initial course of therapy that can be predictive of survival.

Disclosure of Potential Conflicts of Interest

No potential conflicts of interest were disclosed.

Acknowledgments

The authors are grateful to all the patients who participated in this study as well as to their families. In addition, the authors thank David Truong, Dat Vu, and Weber Shao for their computer and database support, the UCLA Cyclotron staff for help with ^{18}F-FLT preparation, and the UCLA Nuclear Medicine staff for assistance with PET acquisition.

Grant Support

This work was supported by the U.S. Department of Energy contract DE-FG02-06ER64249 and the NIH grant P50 CA086306.

The costs of publication of this article were defrayed in part by the payment of page charges. This article must therefore be hereby marked *advertisement* in accordance with 18 U.S.C. Section 1734 solely to indicate this fact.

Received December 12, 2010; revised July 6, 2011; accepted August 11, 2011; published OnlineFirst August 25, 2011.

References

1. Shields AF, Grierson JR, Dohmen BM, Machulla HJ, Stayanoff JC, Lawhorn-Crews JM, et al. Imaging proliferation *in vivo* with [F-18]FLT and positron emission tomography. Nat Med 1998;4:1334–6.
2. Bading JR, Shields AF. Imaging of cell proliferation: status and prospects. J Nucl Med 2008;49:64S–80S.
3. Salskov A, Tammisetti VS, Grierson J, Vesselle H. FLT: measuring tumor cell proliferation *in vivo* with positron emission tomography and 3′-deoxy-3′-[^{18}F]fluorothymidine. Semin Nucl Med 2007;37:429–39.
4. Ullrich R, Backes H, Li H, Kracht L, Miletic H, Kesper K, et al. Glioma proliferation as assessed by 3′-fluoro-3′-deoxy-L-thymidine positron emission tomography in patients with newly diagnosed high-grade glioma. Clin Cancer Res 2008;14:2049–55.
5. Spence AM, Muzi M, Link JM, O'Sullivan F, Eary JF, Hoffman JM, et al. NCI-sponsored trial for the evaluation of safety and preliminary efficacy of 3′-deoxy-3′-[^{18}F]fluorothymidine (FLT) as a marker of proliferation in patients with recurrent gliomas: preliminary efficacy studies. Mol Imaging Biol 2009;11:343–55.
6. Jacobs AH, Thomas A, Kracht LW, Li H, Dittmar C, Garlip G, et al. ^{18}F-Fluoro-L-thymidine and 11C-methylmethionine as markers of increased transport and proliferation in brain tumors. J Nucl Med 2005;46:1948–58.
7. Schiepers C, Chen W, Dahlbom M, Cloughesy T, Hoh CK, Huang SC. ^{18}F-Fluorothymidine kinetics of malignant brain tumors. Eur J Nucl Med Mol Imaging 2007;34:1003–11.

Downloaded from http://aacrjournals.org/clincancerres/article-pdf/17/20/6553/2000121/6553.pdf by guest on 19 June 2024

8. Schiepers C, Chen W, Cloughesy T, Dahlbom M, Huang SC. ^{18}F-FDOPA kinetics in brain tumors. J Nucl Med 2007;48:1651–61.
9. Muzi M, Spence AM, O'Sullivan F, Mankoff DA, Wells JM, Grierson JR, et al. Kinetic analysis of 3′-deoxy-3′-^{18}F-fluorothymidine in patients with gliomas. J Nucl Med 2006;47:1612–21.
10. Schiepers C, Dahlbom M, Chen W, Cloughesy T, Czernin J, Phelps ME, et al. Kinetics of 3′-deoxy-3′-^{18}F-fluorothymidine during treatment monitoring of recurrent high-grade glioma. J Nucl Med 2010;51:720–7.
11. Chen W, Delaloye S, Silverman DH, Geist C, Czernin J, Sayre J, et al. Predicting treatment response of malignant gliomas to bevacizumab and irinotecan by imaging proliferation with [^{18}F]fluorothymidine positron emission tomography: a pilot study. J Clin Oncol 2007;25:4714–21.
12. Galldiks N, Kracht LW, Burghaus L, Thomas A, Jacobs AH, Heiss WD, et al. Use of 11C-methionine PET to monitor the effects of temozolomide chemotherapy in malignant gliomas. Eur J Nucl Med Mol Imaging 2006;33:516–24.
13. Chen W. Clinical applications of PET in brain tumors. J Nucl Med 2007;48:1468–81.
14. Wyss M, Hofer S, Bruehlmeier M, Hefti M, Uhlmann C, Bartschi E, et al. Early metabolic responses in temozolomide treated low-grade glioma patients. J Neurooncol 2009;95:87–93.
15. Pope WB, Kim HJ, Huo J, Alger J, Brown MS, Gjertson D, et al. Recurrent glioblastoma multiforme: ADC histogram analysis predicts response to bevacizumab treatment. Radiology 2009;252:182–9.
16. Dhermain FG, Hau P, Lanfermann H, Jacobs AH, van den Bent MJ. Advanced MRI and PET imaging for assessment of treatment response in patients with gliomas. Lancet Neurol 2010;9:906–20.
17. Ballman KV, Buckner JC, Brown PD, Giannini C, Flynn PJ, LaPlant BR, et al. The relationship between six-month progression-free survival and 12-month overall survival end points for phase II trials in patients with glioblastoma multiforme. Neuro Oncol 2007;9:29–38.
18. Walsh JC, Padgett HC, Ysaguirre T, inventors; Siemens Medical Solutions USA, Inc., assignee. Method for preparing radiolabeled thymidine having low chromophoric byproducts. United States patent US 7419653. 2008 Sept 2.
19. Wu HM, Hoh CK, Choi Y, Schelbert HR, Hawkins RA, Phelps ME, et al. Factor analysis for extraction of blood time-activity curves in dynamic FDG-PET studies. J Nucl Med 1995;36:1714–22.
20. Schiepers C, Hoh CK, Dahlbom M, Wu HM, Phelps ME. Factor analysis for delineation of organ structures, creation of in- and output functions, and standardization of multicenter kinetic modeling. Proc SPIE 1999;3661:1343–50.
21. Sitek A, Di Bella EV, Gullberg GT. Factor analysis with a priori knowledge—application in dynamic cardiac SPECT. Phys Med Biol 2000;45:2619–38.
22. Paproski RJ, Ng AM, Yao SY, Graham K, Young JD, Cass CE. The role of human nucleoside transporters in uptake of 3′-deoxy-3′-fluorothymidine. Mol Pharmacol 2008;74:1372–80.
23. Muzi M, Vesselle H, Grierson JR, Mankoff DA, Schmidt RA, Peterson L, et al. Kinetic analysis of 3′-deoxy-3′-fluorothymidine PET studies: validation studies in patients with lung cancer. J Nucl Med 2005;46:274–82.
24. Muzi M, Mankoff DA, Grierson JR, Wells JM, Vesselle H, Krohn KA. Kinetic modeling of 3′-deoxy-3′-fluorothymidine in somatic tumors: mathematical studies. J Nucl Med 2005;46:371–80.
25. Phelps ME. PET: molecular imaging and its biological applications. New York: Springer; 2004.
26. Afifi AA, Clark V, May S. Computer-aided multivariate analysis. 4th ed. Boca Raton, FL: Chapman & Hall/CRC; 2004.
27. Chan YH. Biostatistics 303. Discriminant analysis. Singapore Med J 2005;46:54–61; quiz 2.
28. Phelps ME. Inaugural article: positron emission tomography provides molecular imaging of biological processes. Proc Natl Acad Sci U S A 2000;97:9226–33.
29. Jain RK, di Tomaso E, Duda DG, Loeffler JS, Sorensen AG, Batchelor TT. Angiogenesis in brain tumours. Nat Rev Neurosci 2007;8:610–22.
30. Chen YL, Eriksson S, Chang ZF. Regulation and functional contribution of thymidine kinase 1 in repair of DNA damage. J Biol Chem 2010;285:27327–35.
31. Nimmagadda S, Shields AF. The role of DNA synthesis imaging in cancer in the era of targeted therapeutics. Cancer Metastasis Rev 2008;27:575–87.
32. Goodman LS, Brunton LL, Blumenthal DK, Murri N, Hilal-Dandan R. Goodman & Gilman's the pharmacological basis of therapeutics. 12th ed. New York: McGraw-Hill Medical; 2011.
33. Szakacs G, Paterson JK, Ludwig JA, Booth-Genthe C, Gottesman MM. Targeting multidrug resistance in cancer. Nat Rev Drug Discov 2006;5:219–34.
34. Loscher W, Potschka H. Drug resistance in brain diseases and the role of drug efflux transporters. Nat Rev Neurosci 2005;6:591–602.
35. Lamborn KR, Yung WK, Chang SM, Wen PY, Cloughesy TF, DeAngelis LM, et al. Progression-free survival: an important end point in evaluating therapy for recurrent high-grade gliomas. Neuro Oncol 2008;10:162–70.

Downloaded from http://aacrjournals.org/clincancerres/article-pdf/17/20/6553/2000121/6553.pdf by guest on 19 June 2024